RSC Advances

ROYAL SOCIETY OF CHEMISTRY

www.rsc.org/advances

Cite this: DOI: 10.1039/c0xx00000x

www.rsc.org/xxxxxx

PAPER

Preparation of Magnetic Calcium Silicate Hydrate for the Efficient Removal of Uranium from Aqueous Systems

Hongsen Zhang[a,b], Qi Liu[a], Jun Wang[*a,c], Jingyuan Liu[a], Huijun Yan[a], Xiaoyan Jing[a], and Bin Zhang[a]

Received (in XXX, XXX) Xth XXXXXXXXX 20XX, Accepted Xth XXXXXXXXX 20XX

DOI: 10.1039/b000000x

To obtain an adsorbent for uranium with superb adsorption capacity, rapid adsorption rate and quick magnetic separation, magnetic calcium silicate hydrate (MCSH) is fabricated through *in situ* growth of calcium silicate hydrate (CSH) onto the surface of the magnetic silica microspheres *via* a sonochemical method. Chemical components, structural and morphological properties of MCSH are characterized by FTIR, XRD, TG, VSM, SEM, TEM and N_2 adsorption-desorption methods. The results show that MCSH with mesoporous structure is constructed by an agglomeration of of CSH nanosheets. The BET specific surface area and saturation magnetization of MCSH are determined to be 196 m^2/g and 15.4 emu/g, respectively. Based on the synthetic MSCH, adsorption isotherms, thermodynamics and kinetics are investigated. The adsorption mechanism fits the Langmuir isotherm model with a maximum adsorption capacity of 2500 mg/g at 298K. The calculated thermodynamic parameters demonstrate that the adsorption process, which is in accordance with a pseudo-second-order model, is spontaneous and endothermic. MCSH exhibits a quick and highly efficient adsorption behavior, and more than 80% of uranium (1000mg/L) is adsorbed in the first 10 min. The superb adsorption capacity and rapid adsorption rate are likely attributed to the ultrahigh specific surface area and facile exchanges of uranium ions and calcium ions of CSH ultrathin nanosheets. These results demonstrate that MSCH is an excellent adsorbent for uranium removal from aqueous systems.

1 Introduction

Uranium is one of the most hazardous contaminants because of its long half-life, high radiological and biological toxicity.[1] Therefore, it is extremely important to choose a suitable and effective method to remove uranium from aqueous systems. In the various processes, adsorption has attracted most interest because of its cost-effectiveness, versatility and simplicity of operation to remove uranium[2]. A number of materials have been developed and modified for adsorption, for example titanium dioxide [3], aluminum oxide [4], magnesium oxide [5], carbon [6], zeolite [7], and layered double hydroxides [8].

Based on the special structure and excellent performance, CSH has shown excellent potential in the safe disposal of low and intermediate level radioactive waste. CSH consists of silica chains connected to CaO sheets and a number of Ca atoms that may be located in the interlayers between the Ca-silicate sheets.[9] The advantages of this adsorbent are as follows: (1) a high surface area containing surface hydroxyl groups and hydrated Ca^{2+} ions to which various chemical entities can be attached or used for ion-exchanged [10,11]; (2) CSH may control the long-term release of radio nuclides because of its long-term stability and high immobilization potential for cations [12]; (3) its low cost, availability, innocuity and environment-friendly nature. Up to date, an increasing interest has been focused on the development of mesoporous CSH due to its larger specific surface area and higher adsorption capacity. For example, the CSH spheres have a well-defined 3D network structure built up by nanosheets, which exhibit ultra-high drug loading capacities.[13] Chitosan-coated CSH mesoporous microspheres are the promising adsorbents and exhibit a quick and highly efficient adsorption behavior toward heavy metal ions.[14]

Unfortunately, CSH is usually a kind of superfine powder, which is easy to lose in the processes of adsorption and difficult to separate from aqueous systems after batch adsorption experiments.[15] As an ideal adsorbent, magnetical materials have attracted extensive interest due to their quick and effective separation from the treated water.[16,17] Among magnetic adsorbents, magnetic mesoporous nanostructures are excellent adsorption materials, because they not only exhibit a high specific surface area owning to the abundant interparticle spaces or intraparticle pores, but also have better magnetic properties than powder adsorbents due to weaker Brownian motion. [18,19] Compared with co-precipitation, sol–gel and hydrothermal methods, the sonochemical method is an excellent method for synthesizing mesoporous nanostructures, because a number of cavitation bubbles resulting from ultrasonic irradiation may contribute to the mesoporous nanostructures of the resulting products, and ultrasound can promote and accelerate some homogeneous chemical reactions.[13] Nevertheless, it is difficult to prepare magnetic hierarchical nanostructures consisting of an

iron oxide core and CSH shell using the conventional method of adding magnetic particles during the process of sonochemical reaction. It is because TEOS rapidly hydrolyzes and reacts with Ca^{2+} cations in basic aqueous solution under ultrasonic irradiation, forming nanosheets of CSH, few of which coat onto magnetic particle surfaces in the self-assembly process. To our knowledge, little work has been reported on magnetic mesoporous CSH as an adsorbent for uranium ion.

In this paper, we report a strategy to prepare an adsorbent consisting of iron oxide core and mesoporous CSH shell (illustrated in Scheme 1). The Ca^{2+} cations are rapidly adsorbed onto the Fe_3O_4@SiO_2 surface *via* electrostatic attraction because the surface of magnetic silica microspheres is full of compact negative charges. In addition, surface modifications of Fe_3O_4 offer an abundance of surface hydroxyl groups to link Ca^{2+} cations. The shell of CSH nanoplatelets forms by an *in situ* growth technique under ultrasonic irradiation. The use of an in situ growth method allows CSH nanoplatelets to become strongly anchored onto the surface of the magnetic core [19]. The magnetic characteristics is helpful for the separation. The core–shell structure renders high specic surface areas.[20] In addition, its application in the removal of uranium from aqueous systems was investigated. The effects of experimental factors on uranium sorption, as well as relevant adsorption kinetics and thermodynamics, were systematically evaluated. The results demonstrate that CSH has high uranium removal efficiency and can be separated quickly from the treated water.

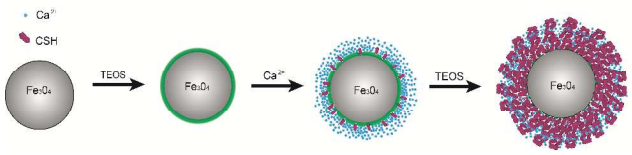

Scheme1. Illustration of the strategy for the preparation of MCS

2. Materials and methods

2.1. Chemicals.

$FeCl_3{\cdot}6H_2O$, $Ca(NO_3)_2{\cdot}4H_2O$, tetraethyl orthosilicate (TEOS), ethanol, and concentrated ammonia solution (28 wt%) were purchased from Tianjin Kemiou Chemical Reagent Company. $UO_2(NO_3)_2{\cdot}6H_2O$ was from Beijing Chemical Reagent Procurement Station of Chinese Pharmaceutical Company. All chemical reagents were of analytical grade and used without further purification.

2.2. Materials for Synthesis of MCSH.

Synthesis of Fe_3O_4/SiO_2 Microspheres. The core-shell Fe_3O_4/SiO_2 microspheres were prepared according to a previous method. [21,22] Typically, $FeCl_3{\cdot}6H_2O$ (2.7g), and sodium acetate (7.2g) were dissolved in ethylene glycol (100 mL) under vigorous stirring. The obtained yellow solution was transferred into a Teflon-lined stainless-steel autoclave, and was heated at 200°C for 8 h. The black product, The obtained Fe_3O_4, was washed with ethanol and deionized water for several times, and dried in vacuum at 60 °C for 12h. Fe_3O_4 (0.10 g) was treated in HCl aqueous solution (50 mL, 0.1M) under ultrasonic vibration for 10 min. Then it was thoroughly washed with deionized water and redispersed in deionized water (20.0 mL). The aqueous dispersion of the magnetite particles was added to a mixture of ethanol (80 mL) and concentrated ammonia solution (1.0 mL, 28 wt %). Afterward, TEOS (30mg) was added dropwise and the reaction allowed to proceed at 30 °C for 6 h. The Fe_3O_4/SiO_2 microspheres were washed with ethanol and water.

Synthesis of MCSH. An aqueous dispersion of the Fe_3O_4/SiO_2 (60 mL, 0.003 g/mL) was added to a three-neck round-bottom flask charged with the solution of $Ca(NO_3)_2$ (100mL, 0.008g/mL), and the reaction mixture was stirred for 10 min at 30°C. NaOH aqueous solution (8.5mL, 1M) and 0.56mL TEOS were separately injected into the resulting mixture. Thereafter, the container was irradiated by ultrasound (ultrasonic cleaner ultrasonic base, 40 kHz, 500 W) for 20 min. The product was separated and collected with a magnet, followed by washing. Finally, the as-prepared sample was freeze-dried overnight.

Synthesis of CSH. In a typical synthetic procedure[13], 5mL 1M NaOH aqueous solution and 0.34mL TEOS were injected into 65mL 0.046M $Ca(NO_3)_2$ aqueous solution. The resulting mixture was ultrasonically irradiated for 20min. The product was separated by centrifugation, washed with ethanol and water, and dried at 60 °C for 3h.

2.3. Characterization

Qualitative chemical structure assessment was done by FT-IR analysis with an AVATAR 360 FT-IR spectrophotometer using a KBr pellet technique. The crystal structure of samples was analyzed by XRD patterns of the solid products, using a Rigaku X-ray powder diffractometer with Cu-Ka radiation (k = 0.154178nm). Morphology was characterized using TEM and SEM. TEM observation was performed on a Tecnai G^2 20 S-TWIN with an accelerating voltage of 200 kV. SEM images were taken by a JEOL JSM-6480 with an energy-dispersive X-ray spectroscopy (EDS) instrument. The magnetic hysteresis loops of samples were measured by a vibrating sample magnetometer (VSM, Lakeshore 7304) at room temperature. Nitrogen adsorption–desorption measurements (BET method) were performed at liquid nitrogen temperature using a micromeritics ASAP 2010 M instrument. The concentrations of uranium ions and calcium ions in the solution were analyzed using ICP-AES (Optima-7000DV).

2.4. Removal of uranium

Uranium removal experiments were performed in a series of conical flasks (100mL) in which a given dose of adsorbents was shaken together with the uranium solution (50mL) of given concentration and pH value in a thermostatic water shaker at speed of 200 rpm. The solution pH was adjusted with 0.5M HNO_3 or NaOH solution. After the sorption reached equilibrium, the solid material was separated out magnetically. The adsorption capacity (q_e mg/g) was calculated using the following equation:

$$q_e = \frac{(C_0 - C_t)V}{W} \quad (1)$$

Where C_0 and C_t are the initial and equilibrium concentration (mg/L), respectively. V is the volume of the solution (L), and W is the mass of MCSH. The adsorption removal efficiency of uranium from aqueous solution was calculated as follows:

$$removal(\%) = \frac{C_o - C_f}{C_o} \times 100 \quad (2)$$

Where C_f is the final concentration (mg/L) of uranium.

3. Results and discussion

3.1 Structural Characterization.

FTIR spectra of Fe_3O_4, Fe_3O_4/SiO_2, and MCSH samples are shown in Figure 1, which is used to characterize the composition of the samples. Across the three samples, a typical Fe-O-Fe vibration of magnetite phase is observed at 580 cm^{-1}, [23] indicating the high content of ferrite in MCSH. After SiO_2 coats onto the surface of Fe_3O_4 nanoparticles (curve b), the characteristic absorption peak at 1086cm^{-1} corresponds to Si-O-Si antisymmetric stretching vibrations.[24] As shown in curve c, a wide and strong peak at about 1054 cm^{-1} is ascribed to the stretching vibration of framework and terminal Si-O-Si groups.[13,25] The characteristic adsorptions at 458 cm^{-1} and 878 cm^{-1} are attributed to Si-O bending vibration .[26]The water molecules and hydroxyl groups of the CSH-phases cause a broad band in 3100-3500 cm^{-1} region as well as an -OH bending mode between 1633 to 1663 cm^{-1}. [27] The bending vibration band at 1633 cm^{-1} has shifted by about 30 cm^{-1} units, which indicates greater restriction due to incorporation or association of water molecules into the host structure. [26] In addition, small amount of $CaCO_3$ is present in MCSH, which is due to the carbonation when exposed to air. Therefore, the 1460 cm^{-1} band is attributed to carbonate stretching modes.

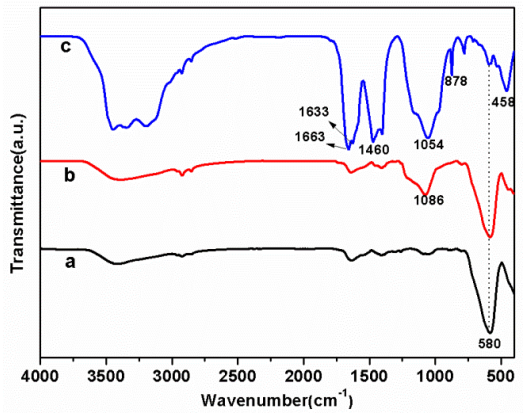

Fig.1 FTIR spectra of Fe_3O_4 (a), Fe_3O_4/SiO_2 (b), and MCSH (c)

The crystal phases of magnetic products are investigated by XRD analysis. Six diffraction peaks (220, 311, 400, 422, 511,and 440) are identified and indexed to the spinal phases for iron oxides, which are in good agreement with Fe_3O_4 (Magnetite, JCPDS19-0629). In Figure 2b and 2c, the sharpness of XRD reflections show that the crystal structure of Fe_3O_4 has not changed after modification with amorphous SiO_2.[28] The XRD pattern of the MCSH (Figure 2C) has a broad peak located at 29.6°due to the unique amorphous nanostructure of CSH, which is similar to the previously reported data for CSH.[13]. Despite decades of research, the precise structure of CSH is still under debate because its complex nature has a poor crystallinity. [29] The limitation on the knowledge of its structure, therefore, has hindered the identification of the CSH adsorption mechanism.

The curve of thermogravimetric analysis (Figure 3) of MCSH is identified by two regions of weight loss. The first region is characterized by a relatively quick weight loss up to 200℃ due to the loss of adsorbed water and crystal water.[30] In the second region, the major weight loss between 200-600℃ is attributed to dehydration of CSH.[29] MCSH exhibits a large amount of water and hydroxyl groups in the structure, most likely due to low overall crystallinity. [30] The results are in agreement with those provided by FTIR and XRD. In addition, the escape of CO_2 increases the mass loss in the range of 550 -600°C. [31]

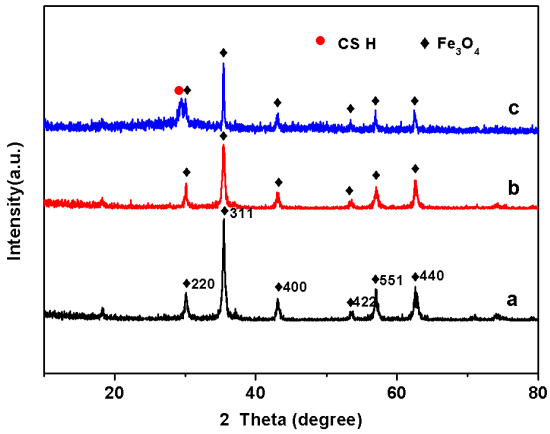

Fig.2 Powder XRD patterns of (a) Fe_3O_4, (b) Fe_3O_4/SiO_2, and (c)MSCH

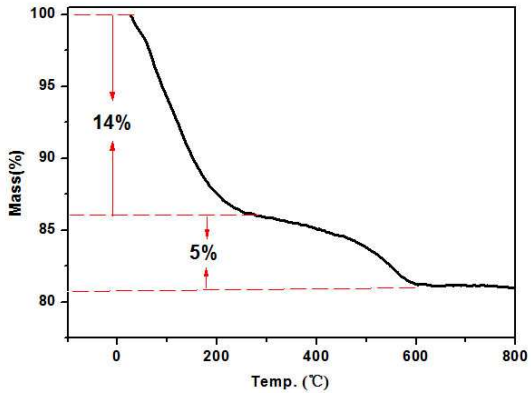

Fig. 3 Curves of thermogravimetric analysis of MSCH

VSM is employed to investigate the magnetic properties of Fe_3O_4 and MCSH, and the magnetic hysteresis loop of the samples is illustrated in Figure 4. The saturation magnetizations of Fe_3O_4 and MCSH are 59.7 and 15.4 emu/g, respectively. The saturation magnetization of MCSH is clearly lower than that of Fe_3O_4, which may be caused by the surface spin canting effects and the surfactant coating reducing the total magnetic moment of nanoparticles. [32,33] Previous research shows that the magnetization value of CNC@Fe_3O_4@SiO_2 decreases with the increasing amounts of TEOS, which indicates that SiO_2 greatly influences the magnetic properties of Fe_3O_4. [34] A simple experiment, in which MCSH from the homogeneous dispersion is attracted to the wall of the vial in 60 s in the presence of an external magnetic field, shows that MCSH retains a high magnetic response in magnetic field to satisfy the need of magnetic separation.

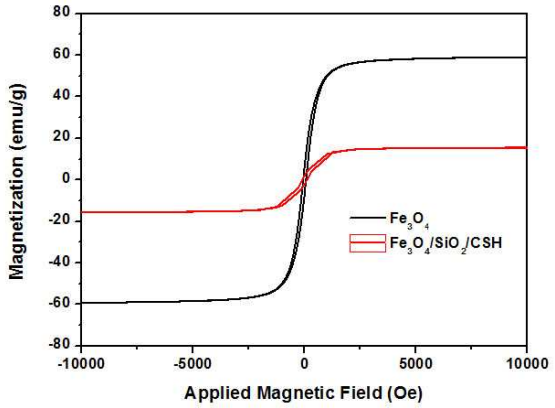

Fig. 4 Room-temperature magnetic hysteresis loops of Fe_3O_4, and MCSH.

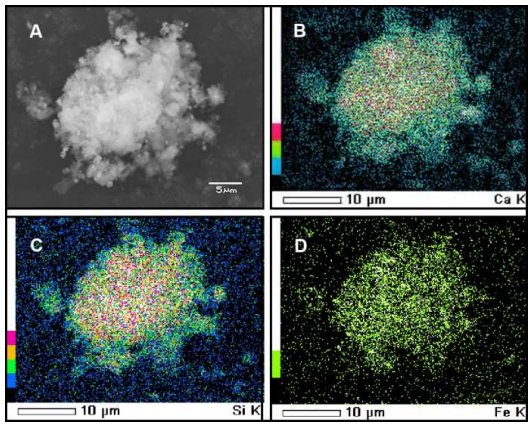

Fig. 5 SEM images ofMCSH (A), EDS mapping of Ca, Si and Fe (B-D)

3.2 Morphological Characterization.

SEM images of MCSH surface are shown in Figure 5A, Ca, Si and Fe maps are displayed in color in Figure 5 B-D. EDS element mappings clearly show homogeneous distributions of Ca, Si and Fe throughout the production. From the TEM images of MCSH (Figure 6), the dark Fe_3O_4 nanoparticles could be clearly observed to be embedded in the light grey CSH. The core of Fe_3O_4 magnetic nanoparticles can be determined to be about 100 nm in diameter, while the entire CSH particles consist of warped thin nanosheets. The nanosheet edges show CSH with a thickness, which is equal to the thickness of a single unit cell of 1.4 nm tobermorite (2.8 nm). This result is consistent with data report previously.[29] The warped ultrathin nanosheets stack together forming nanoporous structures. The structural features of MCSH are highly desirable for uranium removal due to the large specific surface area, mesopores, and interconnected microchannels.

Figure 7 shows typical nitrogen adsorption-desorption isotherm and pore size distribution of MCSH. According to the International Union of Pure and Applied Chemistry (IUPAC) definitions of porosity, the sorption curve of MCSH (Figure 7A) is described as a type H3 hysteresis loop derived from plate-like-particle aggregates with slit-shaped pores, [14,35] which is consistent with the TEM observation. The steep increase at P/P_0 0.9–1.0 in Figure 7A suggests the presence of a macroporous structure [13]. The pore-size-distribution curve (Figure 7B) shows most of the pores are in the range of 5–50nm in diameter, which contribute to most of the pore volume. The Brunauer-Emmett-Teller (BET) is measured to be 196 m^2/g, which is relatively higher than other magnetic materials. The mesoporous structure provides a significantly high specific surface area, high adsorption capacity and fast uptake kinetics, so the mesoporous microspheres are promising adsorbent toward uranium ions[14].

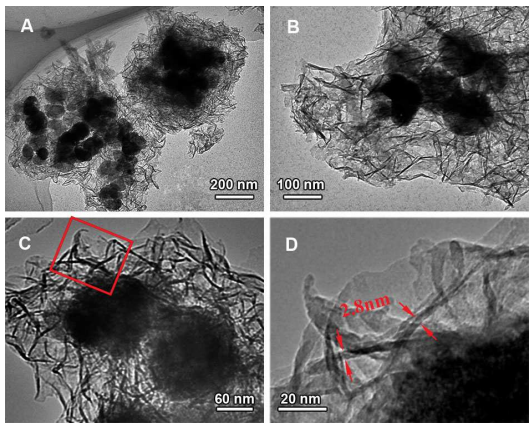

Fig.6 TEM images of MCSH.

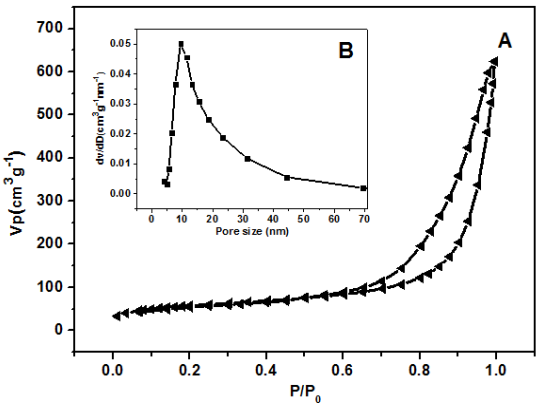

Fig. 7 Nitrogen adsorption–desorption isotherm (A) and BJH-desorption pore size distribution curve (B) of the as-prepared MCSH.

3.3 Application in removal of uranium.

3.3.1 Effect of Initial pH and adsorbent dosage

The pH value of adsorption medium is one of the most important parameters who can influence the chemical properties of uranium and adsorbents [5]. The influence of pH on the adsorption of uranium on MCSH was investigated using 50 mL of uranium 200 mg/L and 0.05g MCSH at pH 2.0–12.0 at 298K for 120 min. In general, common adsorbents have the preferable adsorption capability in very narrow pH regions. [2,8] However, Figure 8 shows high removal efficiencies (96.3-98.9%) and no significant influence of pH on uranium removal for MCSH in the wide range

of pH 4-12. The excellent adsorption ability may be attributed to the fact that CSH exhibits a large number of structural sites available for cation and anion binding [12,36]. The removal rate at pH 8 decreases slightly, which is probably caused by the reduced number of ions. In addition，the removal rate of uranium at pH 2 clearly decreases. To explain this phenomenon，the concentration of calcium ion after adsorption at pH 2 is measured by ICP-AES, and reveals that it is twice larger than that of other pH，indicating CSH structure has been destroyed in part under strong acidic conditions. The focus of interaction of uranium and CSH is usually in high-pH solutions, because the immobilization of low- and intermediate-level radioactive waste in cementitious materials is in highly alkaline conditions. However, the pH values of industrial effluents or wastewaters usually are in the relatively acidic range [37]. Therefore, pH 5 is adopted in further experiments.

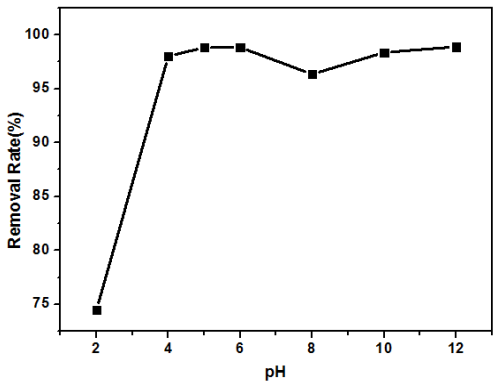

Fig. 8. Effect of pH value on adsorption property of uranium by MCSH. (Adsorption dosage: 0.05 g, C_0 = 200 mg/L, retention time: 120min, T = 298K and pH 2–12).

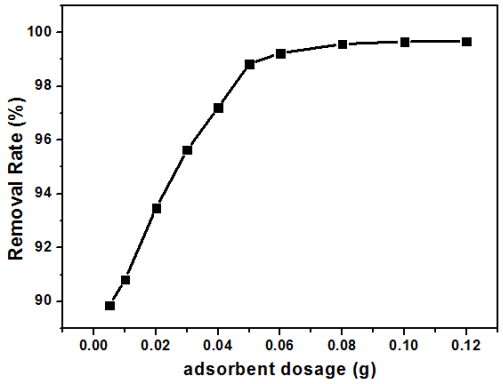

Fig. 9 The effect of adsorbent dosage on the uptake of uranium by MSCH (Adsorption dosage: 0.005–0.120 g, C_0 = 200 mg/L, retention time: 120min, T = 298K and pH 5)

To evaluate the effect of the adsorbent dosage on the adsorption, the removal of uranium by MCSH at different adsorbent dosages (0.005-0.120 g) for the uranium concentration of 200 mg/L at 298K for 120 min is studied. Experimental results (Figure 9) reveal that the removal efficiency of uranium by 0.005g adsorbent is nearly 90%, which suggests that MCSH is a potentially efficient adsorbent for the treatment of waste water with high concentrations of uranium. The percentage of uranium removal approaches equilibrium (99.23%) at a dosage of 0.06 g MCSH. In considering the removal efficiency and the cost, 0.06g is considered as an optimum dosages and is used for further study.

3.3.2 Sorption isotherms

Isotherms studies can describe how adsorbates interact with adsorbents, which is critical in optimizing the use of adsorbent and designing a desired adsorption system [38]. Adsorption isotherms of MCSH at temperatures of 298K and 318K are investigated in varying initial uranium concentration from 50 to 5000 mg/L at the conditions of 60 mg adsorbent, pH 5. Figure 10 shows that the adsorption of uranium increases with the increasing of temperature, which demonstrates that adsorption capacity is enhanced at higher temperatures.

To examine the relationship between absorbed (qe) and aqueous concentration (Ce) of uranium at equilibrium, the Langmuir (eq 3) and Freundlich (eq 4) models are used to describe this adsorption process.

$$\frac{C_e}{q_e} = \frac{1}{Q_m b} + \frac{C_e}{Q_m} \quad (3)$$

$$\log q_e = \log K_F + \frac{1}{n} \log C_e \quad (4)$$

Where b is a equilibrium constant (L/mg), Q_m is the maximum adsorption capacity (mg/g), K_F is an indicator of adsorption capacity, and n is the adsorption intensity. All adsorption data obtained are fitted to both models as shown in Figure S1 and S2. The relative parameters of the Langmuir and Freundlich models were calculated and listed in Table 1. According to the correlation coefficients, we conclude that the Langmuir isotherm is more suitable to characterize the uranium adsorption behavior on MCSH than the Freundlich model. Langmuir isotherm assumes that the uptake of metal ions occurs on a homogeneous surface by monolayer adsorption, and Freundlich isotherm is based on heterogeneous surfaces. Therefore, uranium is adsorbed in the form of a monolayer coverage on the surface of CSH.

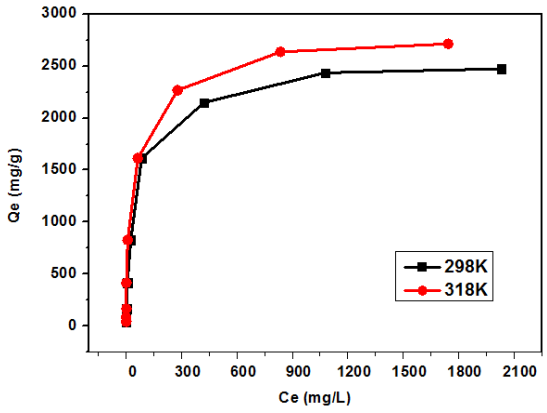

Fig. 10 Effect of uranium concentration on the adsorption of uranium by MCSH. (Adsorption dosage 0.06 g, C_0= 50–5000 mg/L, reaction time 120min, T = 298K and 318K, and pH 5).

Table 1 Isotherm parameters for adsorption of uranium on MSCH

T (K)	Langmuir constants				Freundlich constants		
	Q_m (mg/g)	b (L/g)	K_L (L/mol)	R^2	K_F	n	R^2
298	2500	0.022	5127	0.999	138.8	2.26	0.810
318	2778	0.028	6663	0.999	136.0	2.12	0.826

The maximum adsorption capacity (Q_m) can be evaluated from the slope of the Langmuir plots. Q_m at 298K and 318K are 2500

mg/g and 2778 mg/g, respectively. These two values show MCSH with superb adsorption capacity. Some research suggests that ion exchange plays a key role for heavy metal ion removal in this superior type of adsorption process.[39,40]

The adsorption standard enthalpy ($\Delta H°$), standard entropy ($\Delta S°$) and standard free energy ($\Delta G°$) for uranium adsorption on MCSH base on Eqs. 5-7.

$$K_L = \frac{q_e}{C_e} \quad (5)$$

$$\Delta G^0 = -RT \ln K_L \quad (6)$$

$$\ln K_L = \frac{\Delta S^0}{R} - \frac{\Delta H^0}{RT} \quad (7)$$

where K_L is the Langmuir isotherm constant, R is the gas constant (8.314 J mol^{-1} K^{-1}) and T is the thermodynamic temperature (K). The values of $\Delta H°$ and $\Delta S°$ are calculated from the linear plot of lnK_L. vs $1/T$ (Figure S3) using Van't Hoff equation (Eq.7). The thermodynamic parameters are listed in Table 2. The negative value of $\Delta G°$ reveals that the adsorption is a spontaneous process, and the values of $\Delta G°$ become more negative with elevated temperature indicating that adsorption progresses more favorably at higher temperatures due to a greater driving force of adsorption. The positive value of $\Delta H°$ indicates that the adsorption is endothermic, which also shows that uranium adsorption becomes more favorable at higher temperatures.The positive value of $\Delta S°$ implys that the increased randomness with adsorption of uranium on MCSH probably because the number of desorbed water molecules is larger than that of the adsorbed uranium ion. Therefore, the adsorption of uranium on MCSH is controlled by the positive entropy change. [41]

Table 2. Thermodynamic parameters for adsorption of uranium on MCSH

Temp(K)	ΔG^0 (kJ/mol)	ΔH^0 (kJ/mol)	ΔS^0 (J/mol/K)
298	-21.164		
		10.38	105.92
318	-23.277		

3.3.3 Adsorption kinetics

The residence time of sorption reaction determines the efficiency of sorption[38], so the experiments of time dependence of uranium adsorption are carried out from 3 to 120 min at the conditions of 1000 mg/L uranium, 60 mg adsorbent, pH 5, 298K and 318K. As can be seen in Figure 12, the sorption of uranium ions appears to take place in two distinct steps: an initial very rapid phase in a few minutes, the removal of more than 80% in 10 min, where adsorption is instantaneous by external surface adsorption. The high initial uptake rate is attributed to high surface area and the mesoporous structure of CSH. Based on structural properties, a rapid diffusion of uranium occurs from solution to the external surfaces of adsorbent. A relatively slower second phase occurs in which intraparticle diffusion controls the adsorption rate until finally the metal uptake reaches equilibrium. In the slow phase uranium is presumably adsorbed by the cationic exchange between calcium ions and heavy metal ions, indicating ion exchange is one of the adsorption mechanisms in this case.

To study the kinetic mechanism which controls the adsorption process, the pseudo-first-order model (eq 8) and pseudo-second-order model (eq 9) are used, [39, 40] and the calculated kinetic parameters are given in Table 3.

$$\ln(q_e - q_t) = \ln q_e - k_1 t \quad (8)$$

$$\frac{t}{q_t} = \frac{1}{k_2 q_e^2} + \frac{t}{q_e} \quad (9)$$

where q_e and q_t are the amount of uranium adsorbed (mg/g) at equilibrium and time t (min), respectively; k_1(min^{-1}) and k_2 (g/mg·min) are the pseudo-first-order rate constant and the pseudo-second-order rate constant , respectively. k_1 can be determined from the intercept of a plot of ln(q_e-q_t) *versus* t (Figure S4). Values of k_2 are calculated from the plots of t/q_e *versus* t (Figure S5) for the adsorbent samples.

The correlation coefficients in Table 3 demonstrate that the absorption of uranium follows a pseudo-second-order kinetic model. It is predicted that adsorption behavior involves valence forces through sharing of electrons between metal ions and adsorbent.[41] The calculated value of adsorption capacity is in agreement with the value of experimental adsorption capacity, accordingly the model adopted is reasonable.

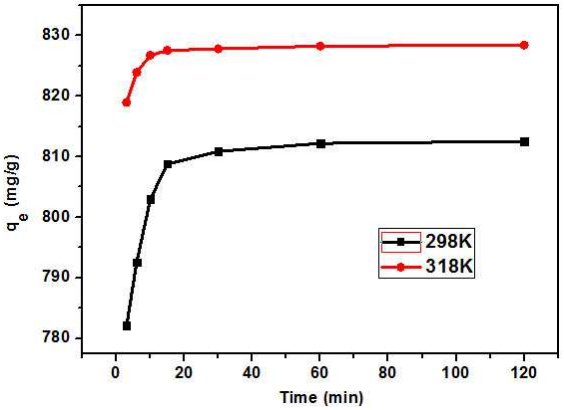

Fig.11. Effect of reaction time on the adsorption of uranium by MSCH (Adsorption dosage 0.06 g, C_0 = 1000 mg/L, reaction time: 3-120 min, T = 298K and 318K, and Ph 5).

Table 3 Kinetic parameters for adsorption of uranium on MCSH

parameters	298K	318K
q_e (exp)	811.78	826.02
Pseudo-first-order		
K_1	0.0001	0.000002
R^2	0.3936	0.3493
q_e(cal)	1703	1959
Pseudo-second-order		
K_2	0.01055	0.04298
R^2	1.0000	1.0000
q_e(cal)	813.01	826.45

3.3.4 Effect of coexisting cations and adsorption mechanism

Natural underground water and wastewater commonly contain other metal cations, which may compete with uranium in the ion exchange process. Furthermore, the effects of coexisting cations on uranium adsorption might be helpful for understanding the adsorption mechanisms. Fig.12 shows the influence of metal cations on uranium adsorption. The concentration of uranium and each of the coexisting ions were maintained at 500 mg/L. The uranium removal rate decreased less than 5% in the presence of Zn^{2+} or Cu^{2+} ions, indicating that these coexisting ions had no remarkable influence on the adsorption of uranium onto MCSH. However, the effect of Al^{3+} ions was larger than that of the other cations. Previous studies have shown that the molecular

environment of adsorbed uranium is mainly dominated by O and Si atoms [46]. It is generally accepted that aluminium can partly replace silicon in the bridging sites of SiO_4 tetrahedra in CSH [47,48]. Therefore, Al^{3+} ions thus have an obvious impact on the uranium adsorption onto CSH due to the change of adsorbent structure. Compared to the experiments without competitive cations, the uranium removal capacities was decreased more than 15% in presence of K^+, Na^+ or Mg^{2+}. Some previous studies reported that alkali ions might be adsorbed in the structure of CSH by the chemical binding force. With the alkali-binding into CSH, Ca/Si ratio in CSH decreased.[49,50] As recent research of the mechanisms of magnesium corrosion shown, magnesium could react with CSH and destroy its durability.[51] The competition between metal ions and uranium for the active adsorption sites does not have seriously impact on its adsorption effect due to the remarkably high adsorption capacities and plentiful active sites of CSH. The structure and composition changes of CSH may dominantly cause the decrease of uranium removal rate.

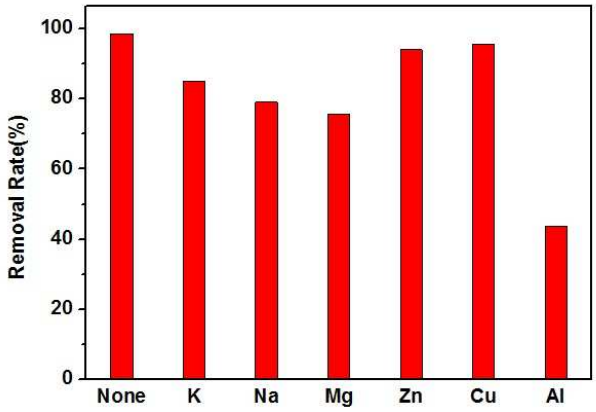

Fig.12 Effect of coexisting ions for uranium onto adsorbent (uranium: 500 mg/L, other ion:500 mg/L,adsorption dosage: 0.006g, retention time: 120min, T = 298K and pH 5).

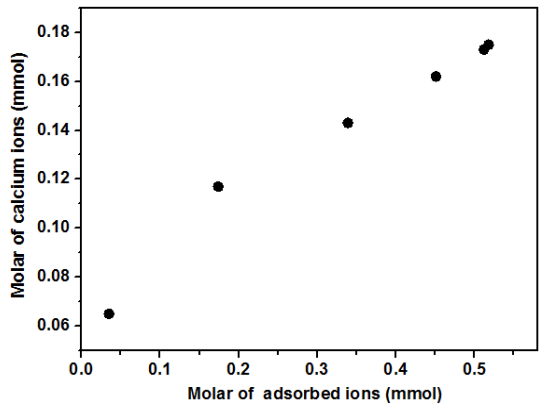

Fig. 13 Molar of exchanged calcium ions vs molar of adsorbed uranium ions. (Adsorption dosage 0.06 g, C_0 = 200–5000 mg/L, reaction time:120min, T = 298K and pH 5).

The ultrahigh specific surface area and large pore volume of CSH are vital factors for high adsorption efficiency and superb adsorption capacity, but the intrinsic nature of adsorbent sometimes is more crucial for the enhancement of absorptive property. The single unit cell of 1.4 nm tobermorite (2.8 nm) has been observed by TEM (Fig.6 D), the structure of which is illustrated in Scheme S1.[29] The double central layer of CaO octahedra is sandwiched between the silicate chains in the tobermorite-like CSH, and the parallel layered structure contains Ca^{2+} ions and water molecules. To further study the adsorption mechanisms, the concentrations of calcium and uranium ions are analyzed. Fig.13 shows a nearly linear relationship of the molar amount of uranium removal and the amount of calcium increment in the solution, which confirms that uranium ions and calcium ions took ion exchange reaction during the adsorption process. CSH possesses the ultrathin nano-structure, which is benefit for the exchange between calcium ions on the surface or in the interlayers and ions in the solution, resulting in high adsorption efficiencies. The charge and ionic radii of Ca^{2+} ion is consistent with those of the adsorbed uranyl ion. The ionic radius of the uranyl ion is only 0.004 nm larger than Ca^{2+}ion[46], which is helpful to retain the structure of CSH during the ion exchange process.

3.3.5 Comparison adsorption capacity between MCSH and CSH

In order to clarify the effect of magnetic iron oxide on the adsorption capacity of CSH, we compared uranium removal rate of MCSH and CSH in different concentrations of uranium. As shown in Fig. 14, the uranium from 200 mg/L to 2000mg/L can be almost entirely adsorbed by two sorbents, suggesting both sorbents with excellent performance in the common concentration range. The amount of uranium loading by CSH decreased slightly when the original concentration levels ranging from 3000 mg/L to 5000 mg/L, and that of MCSH declined rather rapidly. The removal rate of uranium ions is around 59.4 and 88.3% for MCSH and CSH in the concentration of 5000mg/L, respectively. Compared with CSH, magnetic iron oxide has poor adsorption capacity, so the amounts of the active adsorption sites in MCSH are lower than those of CSH. Although CSH has higher adsorption capacities due to more active sites in superb high concentration, such high concentration of uranium is extremely rare in natural underground water and wastewater. CSH and MCSH have almost the same adsorption capacity in the common concentration range, but the magnetic materials can be separated quickly from the treated water.

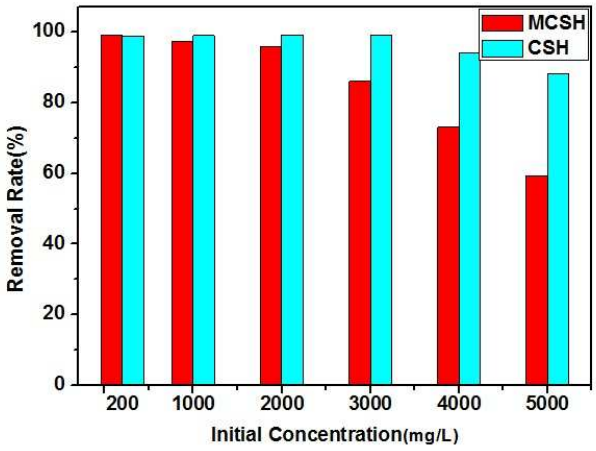

Fig.14 The removal rate of uranium by MCSH and CSH(adsorption dosage: 0.006g, retention time: 120min, T = 298K and pH 5)

4. Conclusions

In summary, MCSH is successfully synthesized through *in situ* growth of CSH onto the surface of the Fe_3O_4@SiO_2 microspheres *via* a sonochemical approach. MCSH has a large surface area and facilitates efficient magnetic separation. The adsorption isotherms are well fitted by the Langmuir model which indicates a monolayer adsorption. MCSH shows superb adsorption capacity (2500 and 2778 mg/g at 298 and 318 K, respectively) with the main adsorption mechanism may be attributed to ion exchange between uranium ions and calcium ions. The adsorption kinetics data are fitted well to the pseudo-second order model. MCSH exhibits a quick and high efficient adsorption behavior, with the removal of more than 80% of uranium (1000mg/L) in 10 min. The calculated thermodynamic parameters demonstrate that this process is spontaneous and exothermic. With the superb adsorption capacity, rapid adsorption rate and quick magnetic separation from the treated water, MCSH has potential as an ideal magnetic adsorbent for uranium removal from aqueous solution.

Acknowledgments

This work was supported by National Natural Science Foundation of China (21353003), Heilongjiang Province Natural Science Funds for Distinguished Young Scholar (JC201404), Innovation Talents of Harbin Science and Technology (2014RFQXJ035), Special Innovation Talents of Harbin Science and Technology for Distinguished Young Scholar (2014RFYXJ005), Natural Science Foundation of Heilongjiang Province (E201329), and the fund for Transformation of Scientific and Technological Achievements of Harbin (2013DB4BG011).

Notes and references

[a] *Key Laboratory of Superlight Material and Surface Technology, Ministry of Education, Harbin Engineering University, Nantong Street 145, PR China. Fax: +86-451-82513026; Tel: +86-451-82533026; E-mail: zhqw1888@sohu.com*

[b] *Modern Analysis, Test and Research Center, Heilongjiang University of Science and Technology, Puyuan Street 2468, Harbin, 150022，PR China.*

[c] *College of Material Science and Chemical Engineering, Harbin Engineering University, Nantong Street 145, Harbin, 150001, PR China.*

† Electronic Supplementary Information (ESI) available: See DOI:10.1039/b000000x/

1 Q.J. Pan, S. O. Odoh, A.M. Asaduzzaman, G. Schreckenbach, *Chem. Eur. J.* 2012, **18**, 1458.

2 H.S. Zhang, J. Wang, B. Zhang, Q. Liu, S.N. Li, H.J. Yan, L.H. Liu, *Colloids and Surfaces A: Physi.* 2014, **444**, 129.

3 M.J. Comarmond, T.E. Payne, J.J. Harrison, S. Thiruvoth, H.K. Wong, R.D. Aughterson, G.R. Lumpkin, K. Müller, H. Foerstendorf, *Environ. Sci. Technol.* 2011, **45**, 5536.

4 Y.Z. Tang, J. Mcdonald, R.J. Reeder, *Environ. Sci. Technol.* 2009, **43** , 4452.

5 H.J. Yan, J.W. Bai, X. Chen, J. Wang, H.S. Zhang, Q. Liu, M.L. Zhang L.H. Liu , *RSC Adv.* 2013, **3**, 23278.

6 G. Tian, J.X. Geng, Y.D. Jin, C.L. Wang, S.Q. Li, Z. Chen, H. Wang, Y.S. Zhao, S.J. Li, *J. Hazard. Mater.* 2011, **190**, 442.

7 L.M. Camacho, S.G. Deng, R.R. Parra, *J.Hazard. Mate.* 2010, **175** ,393.

8 S.N. Li, H.B. Bai, J. Wang, X.Y. Jing, Q. Liu, M.L. Zhang, *Chem. Eng. J.* 2012, **193-194**, 372.

9 J. Tits, G. Geipel, N. Macéa, M. Eilzer, E. Wieland, *J. Colloid Interf. Sci.* 2011, **359**, 248.

10 Y. Kuwahara, S. Tamagawa, T. Fujitania, H. Yamashita, *J. Mater. Chem. A.* 2013, **1**, 7200.

11 X.J. Kang, S.S. Huang, P.P. Yang, P.A. Ma, D.M. Yang, J. Lin, *Dalton Trans.* 2011, **40**, 1878.

12 M. Harfouche，E.Wieland，R.Dähn T. Fujita，J. Tits, D. Kunz, M. Tsukamot, *J. Colloid Interf. Sci.* 2006, **303**, 195.

13 J. Wu, Y.J. Zhu, S.W. Cao, F. Chen. *Adv. Mater.* 2010, **22**, 749-753.

14 J.Zhao, Y.J.Zhu, J. Wu, J.Q. Zheng, X.Y. Zhao, B.Q. Lu, F.Chen, *J. Colloid Interf. Sci.* 2014, **418**, 208-210.

15 S.W. Zhang, J.X. Li, T. Wen, J.Z. Xu, X.K. Wang. *RSC Adv.*, 2013,**3**, 2754.

16 S.W. Zhang, M.Y. Zeng, J.X. Li, J. Li, J.Z. Xu, X.K. Wang. *J. Mater. Chem. A*, 2014, **2**, 4391

17 X.L. Yu, S.R.Tong, M.F. Ge, J.C. Zuo, C.Y. Cao, W.G. Song. *J. Mater. Chem. A*, 2013, **1**, 959

18 I. D.Vicente, A. Merino-Martos, L.Cruz-Pizarro, J.D.Vicente, *J. Hazard. Mater.* 2010, **181**, 376

19 M.F.Shao, F.Y.Ning, J.W.Zhao, M.Wei, D.G.Evans, X.Duan, *J.Am. Chem.Soc.* 2012, **134**, 1072.

20 S.W. Zhang,W.Q. Xu, M.Y. Zeng, J. Li, J.X, Li,*a J.Z. Xu, X.K.Wang *J. Mater. Chem. A*, 2013, **1**, 1169121 Y.H. Deng, D.W. Qi, C.H.Deng, X.M. Zhang, D.Y. Zhao, *J.Am. Chem.Soc.* 2008, **130**, 28.22 S.H Xuan., YX.J. Wang, J.C. Yu, K.CF, *Langmuir*, 2009, **25**, 11836.

23 C. Y. Zhao, A. B. Zhang, Y. P. Zheng, J. F. Luan, *Mater. Res. Bull.* 2012, **47**, 218.

24 Q. Chang, L.H. Zhu , C. Yu, H.Q. Tang, *J. Lumin.* 2008, **128**, 1892.

25 S.H. Chen , Z. Yin , S.L. Luo , C.T. Au , X.J. Li, *Mater. Res. Bull.* 2013, **48**, 727.

26 M.Y.A. Mollah, W.H. Yu, R. Schennach, D.L. Cock, *Cement Concrete Res.* 2000, **30**, 269.

27 A. Hartmann M. Khakhutov J.C, *Mater. Res. Bull.* 2014, **51**, 395.

28 Y.Q. Leng, W.L. Guo, X. Shi, Y.Y. Li, L.T. Xing, *Ind. Eng. Chem. Res.* 2013, **52**, 13609.

29 J. Wu , Y.J. Zhu, F. Chen, *Small*. 2013, **17**, 2911-2925.

30 S. Tränkle, D. Jahn, T. Neumann, L. Nicoleau, N. Hüsing, D. Volkmer, *J. Mater. Chem. A*. 2013, **1**, 10324.

31 A. Morandeau, M. Thiéry, P. Dangla, *Cement Concrete Res.* 2014, **56**, 157.

32 B. Z. Tang, Y. Geng, J. W. Y. Lam, B. Li, X. Jing, X. Wang, F. Wang, A. B. Pakhomov, X. X. Zhang, *Chem. Mater*. 1999, **11**, 1581.

33 H.B. Xia, J.B. Yi, P.S. Foo, B.H. Liu, *Chem. Mater.* 2007, **19**, 4091.

34 L. Chen, R.M. Berry, K.C. Tam, *ACS Sustainable Chem. Eng.* 2014, **4,** 955.

35 K.S.W. Sing, *Pure Appl. Chem.* 1982, **54**, 2211.

36 M. L. D. Gougar, B. E. Scheetz, D. M. Roy, *Waste Manage.* 1996, **16,** 302.

37 L. Zhou, C. Gao, W.J. Xu, *ACS Appl. Mater. Interfaces.* 2010, **2**, 1489.

38 Q. H. Hu, S. Z. Qiao, F. Haghseresht, M. A. Wilson, G. Q. Liu, *Ind. Eng. Chem. Res.* 2006, **45**, 737.

39 C.Y. Cao, P. Li, J. Qu, Z.F. Dou, W.S. Yan, J.F. Zhu, Z.Y. Wu, W.G. Song, *J. Mater. Chem.* 2012, **22**, 19901.

40 C.Y. Cao, J. Qu, F. Wei, H. Liu, W.G. Song, *ACS Appl. Mater. Interfaces.* 2012, **4**, 4286.

41 J.Q. Jiang, C.X. Yang, X.P. Yan, *ACS Appl. Mater. Interfaces* 2013, **5**, 9841.

42 P. Llaiyaraja, A. K. S. Deb, K. Sivasubramanian, D. Ponraju, B. Venkatraman, *J. Hazard. Mater.* 2013, **250-251**, 160.

43 Y.S. Ho, *J. Hazard. Mater.* 2006, **136**, 681–689

44 Y.S. Ho, G. McKay, *Chem. Eng. J.* 1998, **70**, 115-124

45 G.H. Wang, J.S. Liu, X.G.Wang, Z.Y. Xie, N.S. Deng, *J. Hazard. Mater.* 2009, **168**, 1057

46 X. Gaona, D. A. Kulik, N. Macé, E. Wieland. *Appl. Geochem.* 2012,**27**, 8347 X.L. Pardal, F. Brunet, T. Charpentier, I. Pochard, A. Nonat *Inorg. Chem*. 2012, **51**, 1835

48 J. Skibsted, M. D. Andersen. *J. Am. Ceram. Soc.*, 2013 **96,** 651

49 Y.M.Tang, Y.F.Miao, Y. Zuo, G.D.Zhang, C.L.Wang. *Constr. Build. Mater.* 2012,**30**,253

50 S.Y.Hong, F.P.Glasser. *Cem. Concr. Res.* 1999,**29**,1893

51 L. E. Nicklaus, M. A. Caffaro, R.W. Fuessle, M.A. Taylor. *Environ. Prog. Sustain.* 2014.**33** 437

Graphical abstract

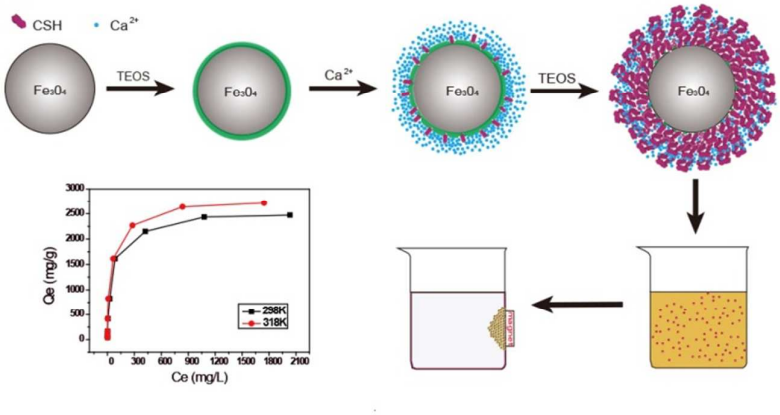

Preparation of a magnetic adsorbent for uranium with rapidly and effectively adsorption characteristics via sonochemical and in-situ growth method.